American Mineralogist, Volume 90, pages 1784–1792, 2005

Crystal chemistry of the elbaite-schorl series

FERDINANDO BOSI,* GIOVANNI B. ANDREOZZI, MARCELLA FEDERICO, GIORGIO GRAZIANI, AND SERGIO LUCCHESI

Dipartimento di Scienze della Terra, Università degli Studi di Roma "La Sapienza" Piazzale A. Moro 5, 00185 Roma, Italy

ABSTRACT

The crystal-chemistry of 13 elbaite-schorl tourmaline crystals from the Cruzeiro pegmatite (Minas Gerais, Brazil) was studied with a multi-analytical approach (SREF, EMPA, SIMS, MS). Effective cation radii at the Y and Z sites and site populations were refined by a minimization procedure. The results indicate that the crystals belong to the alkali group. Elbaite crystals are O^{2-}-free at the W and V sites and show OH content at the O2 site (up to 0.2 apfu). Conversely, schorl crystals always show O^{2-} at the W site. The main substitutional mechanism is the dehydroxylation type:

$$^{Y}Fe^{2+} + {}^{Y}Fe^{3+} + {}^{W}O \rightarrow {}^{Y}Li + {}^{Y}Al + {}^{W}(OH+F).$$

The T site is characterized by $^{T}Si \rightarrow {}^{T}Al$ substitution. <X-O> is linearly correlated with vacancy content in crystals with (OH + F) ≤ 4, whereas it is almost constant in crystals with OH at the O2 position. Along the series, <Y-O> is inversely correlated with ^{Y}Al. The Z site is almost fully occupied by R^{3+} (with ^{Z}Al largely dominant) and the $^{Z}Fe_{tot} \leftrightarrow {}^{Z}Al$ substitution explains the inverse correlation of <Z-O> with ^{Z}Al.

In the elbaite compositional range, lattice parameters are functions of <Y-O>, whereas in the schorl range they are essentially functions of <Z-O>. Along the whole elbaite-schorl series, both chemical substitutions and size increase of Y are far larger than those of Z. In spite of this, lattice parameters increase with <Y-O> as much as with <Z-O>. This is due to the role of the $[ZO_6]$ polyhedra, which extend along **a** and **c** to form the skeleton of the tourmaline structure. Therefore, any change in the size of Z leads to a change in the whole structure.

INTRODUCTION

Minerals of the tourmaline group occur in most crustal environments, from igneous to metamorphic, metasomatic, and occasionally sedimentary. Being the most geologically widespread borosilicate phase it has been extensively studied, the focus being mainly on its complex crystal chemistry.

The general formula can be written as $XY_3Z_6[T_6O_{18}](BO_3)_3V_3W$, where: X = Ca, Na, K, □; Y = Li, Mg, Fe^{2+}, Mn^{2+}, Zn, Al, Cr^{3+}, V^{3+}, Fe^{3+}, Ti^{4+}; Z = Mg, Al, Fe^{2+}, Fe^{3+}, Cr^{3+}, V^{3+}; T = Si, Al, B; B = B, (□); V = OH, O; W = OH, F, O. Thus, the structure allows many substitutions which result in numerous end-members and make the crystal chemistry difficult to characterize fully. One of the major problems in defining the relationships among polyhedral size, unit-cell parameters, and crystal-chemical properties are ion site assignments, which are not straightforward. To overcome this difficulty, some recent crystal-chemical studies have focused on chemically defined series such as schorl-dravite (Bosi and Lucchesi 2004), dravite-chromdravite (Bosi et al. 2004), and Mn-rich tourmaline (Bosi et al. 2005). For the elbaite-schorl series, no systematic study has ever been carried out, and knowledge is still limited to a few end-member structure determinations (e.g., Donnay and Barton 1972; Fortier and Donnay 1975; Grice and Ercit 1993; Cámara et al. 2002). This paper is an attempt to fill this void. With this aim, tourmaline crystals from a petrologically well-characterized environment, the Cruzeiro pegmatite in Brazil, were examined because they feature chemical compositions that almost completely span the elbaite-schorl series and are characterized by internal genetic unity.

SAMPLE OCCURRENCE

The Cruzeiro pegmatite is located in the Brazilian state of Minas Gerais and is included in a metamorphic series of Proterozoic age known as the "schist-quartzite sequence". This sequence constitutes the topographic elevation of Serra da Safira, at the top of which outcrop thick layers of coarse-grained quartzite containing the lens-shaped dikes of the Cruzeiro pegmatite. For a full description of the geological setting, see Federico et al. (1998) and references therein.

This Li-, B-, Be-, Nb-, Ta-, and Zn-enriched miarolitic pegmatite consists of three internally zoned dikes. In particular, the internal zoning of dike 1, as described in Federico et al. (1998), is highlighted by different coexisting mineral assemblages (mainly albite, muscovite, quartz, and minor tourmaline) which define five zones (internal, medium and external intermediate, wall, and border) symmetrically distributed around a central quartz core. Tourmaline crystals are ubiquitous, but are particularly

* E-mail: ferdinando.bosi@uniroma1.it

0003-004X/05/1112–1784$05.00/DOI: 10.2138/am.2005.1827

abundant in the inner zones and in pockets, which are randomly distributed between the internal intermediate zone and the quartz core, and show marked chemical dependence on the evolution of the pegmatite. An extensive chemical study (Federico et al. 1998) clarified the substitution mechanisms operating in Cruzeiro tourmalines. The elbaite-schorl tourmalines described in this paper were collected along the Joao de Matos adit of dike 1 (Table 1). The Mg-schorl crystals (L2al, L2ap, L4aa, L3l) from the outer zones were studied by Bosi and Lucchesi (2004).

Experimental method

X-ray diffraction

Thirteen crystals representative of the elbaite-schorl series were selected from almost 100 tourmaline equidimensional fragments collected from various zones of the pegmatite. After preliminary optical examination, X-ray data collection (Table 2) was carried out with a Siemens *P*4 automated four-circle diffractometer. Cell parameters (Table 3) were measured using 52 reflections (13 independent and their Friedel pairs, on both sides of the direct beam). The scan speed was variable, depending on reflection intensity, estimated with a pre-scan. The background was measured with a stationary crystal and counter at the beginning and end of each scan, in both cases for half the scan time. Preliminary full exploration of reciprocal space was carried out and no violations of *R*3*m* symmetry were noted.

Data reduction was performed with the SHELXTL-PC program. The intensities were corrected for Lorentz and polarization effects. Absorption corrections were made with a semi-empirical method, using 13 Ψ scans (from 10° to 95° 2θ). Only reflections with $I > 2\sigma(I)$ were used (Table 3) from the original set of 3416–3521 data, in a full-matrix least-squares refinement, with unitary weights, in the *R*3*m* space group. The absolute configuration was evaluated according to Barton (1969) and starting coordinates were taken from Foit (1989). The variable parameters were: scale factor, isotropic secondary extinction coefficient, atomic coordinates, site scattering values expressed as mean atomic number (m.a.n.) of the X, Y, Z, B and T sites, and displacement factors (Tables 3 and 4). No chemical constraints were applied during refinement. Scattering curves for neutral B, 50% ionized Si, Al, and O, fully ionized Fe^{2+}, Li, Na, and F were used, because they furnished the best values of conventional agreement factors over all $\sin\theta/\lambda$ intervals. The occupancies of Y site were obtained by considering the presence of Al vs. Li for elbaite and Al vs. Fe^{2+} for schorl crystals. The occupancy of Z site in the schorl crystals was obtained by considering Al vs. Fe^{2+}. The H atom associated with O3 (H3) was found by difference Fourier synthesis for most crystals, and subsequently refined. Three cycles with isotropic thermal factors were followed by anisotropic cycles, until convergence was obtained to satisfactory *R* values of 2.00–3.67% (Table 3).

Table 1. Location of tourmaline in various zones of the Cruzeiro pegmatite, dike 1

Zones	Crystal
Pocket	66c, 61Rda, 60fc, 62ha, 64gh, 61Vbh
Internal Intermediate	L4e
Medium Intermediate	L4c, L4b, L4d
External Intermediate	L3h
Border	L1v, L1z

Table 2. Parameters for X-ray data collection

Determination of unit-cell parameters	
Radiation	Mo$K\alpha_1$ (0.70930 Å)
Reflections used	13 (Friedel pairs on both +2θ and –2θ)
Range	85° – 95° 2θ
Temperature	296 K
Diffraction intensity collection	
Radiation	Mo$K\alpha$ (0.71073 Å)
Monochromator	High crystallinity graphite crystal
Range	3° – 95° 2θ
Reciprocal space range	$0 \le h, k \le 34$ $-15 \le l \le 15$
Scan method	ω
Scan range	2.4° 2θ
Scan speed	Variable 2.93° – 29.30° 2θ/min
Temperature	296 K

These values are in good agreement with those expected for tourmaline with data collection up to ~95° 2θ (Foit 1989). The U_{eq} values for O1 are higher than those for the other anion sites. This could be related to positional disorder rather than thermal vibration (Burns et al. 1994). Mean bond distances and site m.a.n. are listed in Table 5. Tables of anisotropic displacement factors and of observed and calculated structure factors may be obtained from the authors upon request.

EMP and SIMS analysis

After X-ray data collection, the same crystals were mounted on glass slides, polished and carbon-coated for electron microprobe analysis (WDS-EDS method) with a CAMECA SX50 electron microprobe, operating at 15 kV and 15 nA (sample current) and with a beam diameter of 5 µm. Raw data were reduced using the ZAF program. The following natural and synthetic standards were used: wollastonite (Si,Ca), jadeite (Al,Na), magnetite (Fe), periclase (Mg), rutile (Ti), orthoclase (K), fluor-phlogopite (F), and metallic Mn and Zn. Each element determination was accepted after checking that the intensity of the analyzed standard before and after each determination was identical within 1%. Ten to 15 spot analyses were performed for each specimen along two orthogonal traverses and mean values are listed in Table 6.

Concentrations of Li, B, and H (Table 6) were determined from the same fragments by SIMS (Secondary Ion Mass Spectrometry), using a Cameca IMS 3f instrument at the "Centre de Recherches Pétrographiques et Géochimiques" (C.N.R.S., Nancy, France). The experimental conditions were as follows: primary current of oxygen negative ions with an intensity of 5 nA, focused on 10 µm; secondary current of positive ions; voltage offset –60 V; energy window 10 V. Measurements were carried out with an electron multiplier in counting mode and with automatic centering of the magnetic field (Deloule et al. 1992). Be, C, and N were checked to establish whether their contents were significant for possible substitutions at the tourmaline sites. However, the results did not support this conjecture, as the Be content reached only a maximum of 15 ppm, and C and N were practically absent. The details of each element calibration may be found in Federico et al. (1998).

^{57}Fe Mössbauer spectroscopy

Mössbauer spectra were collected at 25 °C using a conventional spectrometer system operating in constant acceleration mode with a ^{57}Co source of 50 mCi in a rhodium matrix. Absorbers were prepared by pressing finely ground samples with a powdered acrylic resin (transoptic powder) to self-supporting disks. For the various samples, from 10 to 60 mg of tourmaline powder were used, depending on both sample availability and total iron contents, so as to have absorbers with an Fe thickness of 1–2 mg/cm^2. The data collection time was usually 1–2 days, but in a few cases spectra had to be collected for one week for good statistics. Spectral data for the velocity range –4 to +4 mm/s were recorded on a multichannel analyzer using 512 channels. After velocity calibration against a spectrum of high-purity α-iron foil (25 mm thick), the raw data were folded to 256 channels. The spectra were fitted assuming Lorentzian peak shapes using the Recoil 1.04 fitting program (Lagarec and Rancourt 1998). Reduced χ^2 was used as a parameter to evaluate statistical best fit, and uncertainties were calculated using the covariance matrix. Errors were estimated at about ±0.02 mm/s for center shift, quadrupole splitting, and peak width, and no less than ±3% for doublet areas. Hyperfine parameters and full discussion of the spectra will be published elsewhere (Andreozzi et al.

Table 3. Crystal data and refinement information for the Cruzerio tourmaline

Crystal	*a* (Å)	*c* (Å)	*V* (Å^3)	No. refl.	Ext.	R_{obs}(%)	GooF
66c	15.8318(6)	7.0998(3)	1541.12(13)	3241	400(9)	2.31	1.306
61Rda	15.8343(8)	7.1007(4)	1541.81(18)	3274	28(3)	2.00	1.238
60fc	15.8468(6)	7.1058(3)	1545.35(13)	3222	55(4)	2.40	1.213
62ha	15.8528(8)	7.1083(5)	1547.06(19)	3265	73(4)	2.17	1.254
64gh	15.8801(6)	7.1169(3)	1554.28(13)	3262	476(10)	2.58	1.431
L4e	15.9010(6)	7.1238(3)	1559.88(13)	3139	94(5)	3.43	1.400
61Vbh	15.9285(6)	7.1286(3)	1566.33(14)	3228	36(3)	3.07	1.354
L4c	15.9569(6)	7.1369(3)	1573.76(14)	3268	381(8)	2.67	1.240
L3h	15.9784(6)	7.1495(4)	1580.79(15)	3009	132(5)	3.67	1.244
L4b	15.9658(6)	7.1487(3)	1578.12(14)	3098	342(7)	3.21	1.130
L4d	15.9768(5)	7.1534(3)	1581.33(12)	3245	257(6)	2.83	1.179
L1v	15.9825(6)	7.1596(3)	1583.83(14)	3170	48(3)	2.77	1.100
L1z	15.9842(6)	7.1581(3)	1583.84(14)	3232	86(4)	2.90	1.343

Notes: no. refl. = number of observed independent reflections; Ext. = Isotropic secondary extinction coefficient (×10^5); $R_{obs} = (\Sigma|F_{obs} - F_{calc}|)/(\Sigma F_{obs})$; GooF = goodness of fit.

TABLE 4. Atomic coordinates and equivalent isotropic *U* values for atoms in the Cruzeiro tourmaline

Atom		66c	61Rda	60fc	62ha	64gh	L4e	61Vbh
X	*x*	0	0	0	0	0	0	0
	y	0	0	0	0	0	0	0
	z	0.23136(32)	0.23271(24)	0.23498(26)	0.23367(23)	0.23458(24)	0.23646(28)	0.23439(29)
	U_{eq}	0.0213(6)	0.0184(4)	0.0211(5)	0.0196(4)	0.0193(4)	0.0209(5)	0.0230(6)
Y	*x*	0.12312(4)	0.12327(4)	0.12331(4)	0.12318(4)	0.12328(4)	0.12393(4)	0.12429(3)
	y	½ *x*	½ *x*	½ *x*	½ *x*	½ *x*	½ *x*	½ *x*
	z	0.63440(9)	0.63436(8)	0.63199(8)	0.63221(8)	0.62898(8)	0.62863(8)	0.62729(7)
	U_{eq}	0.0067(2)	0.0065(1)	0.0060(1)	0.0065(1)	0.0070(1)	0.0066(1)	0.0069(1)
Z	*x*	0.29670(2)	0.29672(2)	0.29690(2)	0.29691(2)	0.29727(2)	0.29760(3)	0.29790(2)
	y	0.25987(2)	0.25987(2)	0.26012(2)	0.26007(2)	0.26053(2)	0.26078(3)	0.26104(2)
	z	0.60996(5)	0.61011(4)	0.61026(5)	0.61051(4)	0.61095(5)	0.61160(7)	0.61145(6)
	U_{eq}	0.00524(7)	0.00498(6)	0.00460(7)	0.00496(7)	0.00537(8)	0.0048(1)	0.0049(1)
B	*x*	0.10903(4)	0.10906(4)	0.10914(4)	0.10919(4)	0.10940(5)	0.10953(7)	0.10980(6)
	y	2*x*	2*x*	2*x*	2*x*	2*x*	2*x*	2*x*
	z	0.45468(16)	0.45484(14)	0.45492(17)	0.45486(15)	0.45466(18)	0.45520(25)	0.45534(22)
	U_{eq}	0.0051(3)	0.0055(2)	0.0048(2)	0.0056(2)	0.0059(3)	0.0049(4)	0.0053(4)
T	*x*	0.19197(1)	0.19196(1)	0.19191(1)	0.19197(1)	0.19195(2)	0.19196(2)	0.19201(2)
	y	0.18988(1)	0.18989(1)	0.18985(2)	0.18992(1)	0.18993(2)	0.18993(2)	0.18998(2)
	z	0	0	0	0	0	0	0
	U_{eq}	0.00416(6)	0.00391(5)	0.00358(6)	0.00389(5)	0.00428(6)	0.00379(9)	0.00378(8)
O1	*x*	0	0	0	0	0	0	0
	y	0	0	0	0	0	0	0
	z	0.78239(30)	0.78265(27)	0.78146(33)	0.78347(31)	0.78274(36)	0.78432(48)	0.78365(46)
	U_{eq}	0.0409(7)	0.0386(7)	0.0450(9)	0.0460(9)	0.055(1)	0.059(2)	0.061(2)
O2	*x*	0.06015(3)	0.06017(3)	0.06032(3)	0.06033(3)	0.06057(4)	0.06071(5)	0.06107(5)
	y	2*x*	2*x*	2*x*	2*x*	2*x*	2*x*	2*x*
	z	0.48966(14)	0.48937(12)	0.48814(15)	0.48778(14)	0.48512(18)	0.48468(21)	0.48478(20)
	U_{eq}	0.0141(2)	0.0143(2)	0.0139(3)	0.0151(2)	0.0177(3)	0.0158(4)	0.0167(4)
O3	*x*	0.26544(8)	0.26567(7)	0.26605(9)	0.26666(8)	0.26771(9)	0.26879(11)	0.26901(10)
	y	½ *x*	½ *x*	½ *x*	½ *x*	½ *x*	½ *x*	½ *x*
	z	0.50744(12)	0.50772(10)	0.50807(13)	0.50809(11)	0.50884(14)	0.50970(18)	0.50937(17)
	U_{eq}	0.0115(3)	0.0112(2)	0.0111(3)	0.0111(2)	0.0110(3)	0.0088(3)	0.0093(3)
O4	*x*	0.09365(3)	0.09354(3)	0.09350(3)	0.09343(3)	0.09334(4)	0.09314(5)	0.09325(4)
	y	2*x*	2*x*	2*x*	2*x*	2*x*	2*x*	2*x*
	z	0.07309(12)	0.07289(10)	0.07286(12)	0.07244(11)	0.07194(13)	0.07146(18)	0.07042(16)
	U_{eq}	0.0078(2)	0.0075(2)	0.0072(2)	0.0075(2)	0.0078(2)	0.0075(3)	0.0077(3)
O5	*x*	0.18746(7)	0.18713(6)	0.18711(7)	0.18702(6)	0.18687(8)	0.18650(10)	0.18689(9)
	y	½ *x*	½ *x*	½ *x*	½ *x*	½ *x*	½ *x*	½ *x*
	z	0.09545(11)	0.09540(10)	0.09511(12)	0.09466(11)	0.09427(13)	0.09367(18)	0.09308(16)
	U_{eq}	0.0079(2)	0.0078(2)	0.0074(2)	0.0076(2)	0.0080(2)	0.0079(3)	0.0081(3)
O6	*x*	0.19541(4)	0.19543(3)	0.19578(4)	0.19586(4)	0.19647(5)	0.19699(6)	0.19751(6)
	y	0.18490(4)	0.18500(4)	0.18530(4)	0.18550(4)	0.18611(5)	0.18687(6)	0.18714(6)
	z	0.77503(8)	0.77522(7)	0.77522(8)	0.77525(7)	0.77540(9)	0.77585(12)	0.77552(11)
	U_{eq}	0.0066(1)	0.0064(1)	0.0061(2)	0.0066(1)	0.0067(2)	0.0065(2)	0.0064(2)
O7	*x*	0.28626(4)	0.28621(3)	0.28610(4)	0.28603(4)	0.28589(4)	0.28563(6)	0.28561(5)
	y	0.28609(4)	0.28605(3)	0.28603(4)	0.28599(4)	0.28598(4)	0.28584(6)	0.28584(5)
	z	0.07879(8)	0.07882(7)	0.07908(8)	0.07939(7)	0.07977(9)	0.08045(12)	0.08028(11)
	U_{eq}	0.0057(1)	0.0054(1)	0.0050(1)	0.0055(1)	0.0057(2)	0.0054(2)	0.0056(2)
O8	*x*	0.20937(4)	0.20944(3)	0.20954(4)	0.20958(4)	0.20980(5)	0.20995(6)	0.20992(6)
	y	0.26983(4)	0.26987(4)	0.27012(4)	0.27010(4)	0.27043(5)	0.27049(7)	0.27047(6)
	z	0.43938(9)	0.43952(7)	0.43987(9)	0.44007(8)	0.44074(10)	0.44164(13)	0.44139(12)
	U_{eq}	0.0070(1)	0.0067(1)	0.0063(2)	0.0068(1)	0.0071(2)	0.0067(2)	0.0069(2)
H3	*x*	-	0.259(3)	0.254(3)	0.258(2)	0.266(3)	-	-
	y	-	½ *x*	½ *x*	½ *x*	½ *x*	-	-
	z	-	0.357(5)	0.355(8)	0.373(4)	0.385(5)	-	-
	U_{eq}	-	0.18(2)	0.08(1)	0.08(1)	0.04(1)	-	-

in preparation).

Inspection of Mössbauer spectra indicated that Fe^{2+} was the principal cation, followed by Fe^{3+} and $Fe^{2.5+}$, and that all iron was in octahedral coordination (Andreozzi et al. 2002). The FeO and Fe_2O_3 contents (Table 6) were obtained from Fe^{2+}/Fe^{3+} ratios measured by Mössbauer spectroscopy. A very satisfactory match was observed between total m.a.n. derived from chemical data and that obtained by structural refinement, as for all crystals the ratio was close to one (Table 6). In a few cases (60fc, L4e, L3h, L1v, and L1z), there was insufficient material to perform Mössbauer analysis, so Fe^{2+}/Fe^{3+} ratios were calculated on the basis of the best match between total scattering values obtained by structural refinement and chemical analysis. Based on previous work with borosilicates (Andreozzi et al. 2000), Fe^{2+}/Fe^{3+} ratios calculated with this procedure are considered to be reliable within ±20% relative.

TABLE 4.—*Continued*

L4c	L3h	L4b	L4d	L1v	L1z
0	0	0	0	0	0
0	0	0	0	0	0
0.23011(37)	0.22524(52)	0.22748(45)	0.22648(44)	0.22594(35)	0.22528(38)
0.0241(7)	0.024(1)	0.0234(9)	0.0228(8)	0.0209(6)	0.0203(7)
0.12462(2)	0.12441(3)	0.12424(3)	0.12429(2)	0.12452(2)	0.12454(2)
½ *x*	½ *x*	½ *x*	½ *x*	½ *x*	½ *x*
0.62638(6)	0.62765(8)	0.62749(6)	0.62778(5)	0.62843(6)	0.62850(6)
0.00763(8)	0.0085(1)	0.00755(9)	0.00759(7)	0.00786(8)	0.00805(8)
0.29823(2)	0.29841(3)	0.29832(3)	0.29840(2)	0.29850(2)	0.29848(2)
0.26135(2)	0.26156(3)	0.26140(3)	0.26155(2)	0.26164(2)	0.26167(2)
0.61087(6)	0.61074(8)	0.61065(7)	0.61057(6)	0.61093(6)	0.61089(6)
0.00470(9)	0.0054(1)	0.0048(1)	0.00447(9)	0.0048(1)	0.0049(1)
0.11008(5)	0.11023(9)	0.11013(7)	0.11032(6)	0.11030(6)	0.11022(6)
2*x*	2*x*	2*x*	2*x*	2*x*	2*x*
0.45477(21)	0.45497(33)	0.45520(26)	0.45469(22)	0.45479(23)	0.45450(25)
0.0052(4)	0.0062(5)	0.0054(5)	0.0052(4)	0.0049(4)	0.0054(4)
0.19199(2)	0.19199(3)	0.19190(2)	0.19196(2)	0.19200(2)	0.19198(2)
0.18995(2)	0.18992(3)	0.18991(2)	0.18992(2)	0.18999(2)	0.18997(2)
0	0	0	0	0	0
0.00393(7)	0.0048(1)	0.0040(1)	0.00387(8)	0.00399(8)	0.00428(9)
0	0	0	0	0	0
0	0	0	0	0	0
0.78192(43)	0.78194(65)	0.78097(53)	0.78056(44)	0.78131(44)	0.78150(47)
0.054(1)	0.051(2)	0.045(1)	0.039(1)	0.042(1)	0.040(1)
0.06141(4)	0.06164(7)	0.06147(5)	0.06170(4)	0.06154(5)	0.06159(5)
2*x*	2*x*	2*x*	2*x*	2*x*	2*x*
0.48586(18)	0.48594(27)	0.48621(22)	0.48699(19)	0.48544(19)	0.48544(20)
0.0165(3)	0.0159(5)	0.0152(4)	0.0146(3)	0.0145(3)	0.0139(4)
0.26884(10)	0.26832(14)	0.26860(12)	0.26807(10)	0.26866(11)	0.26860(11)
½ *x*	½ *x*	½ *x*	½ *x*	½ *x*	½ *x*
0.50927(16)	0.50951(24)	0.50962(20)	0.50941(17)	0.50964(17)	0.50965(18)
0.0101(3)	0.0112(5)	0.0104(4)	0.0111(3)	0.0109(3)	0.0108(4)
0.09339(4)	0.09332(6)	0.09339(5)	0.09342(4)	0.09317(5)	0.09318(5)
2*x*	2*x*	2*x*	2*x*	2*x*	2*x*
0.06920(15)	0.06841(23)	0.06905(19)	0.06841(16)	0.06864(16)	0.06852(18)
0.0081(3)	0.0094(4)	0.0086(3)	0.0084(3)	0.0088(3)	0.0088(3)
0.18728(9)	0.18760(13)	0.18714(11)	0.18750(9)	0.18676(9)	0.18686(10)
½ *x*	½ *x*	½ *x*	½ *x*	½ *x*	½ *x*
0.09203(15)	0.09145(24)	0.09126(19)	0.09164(16)	0.09128(17)	0.09141(18)
0.0084(3)	0.0098(4)	0.0085(3)	0.0086(3)	0.0089(3)	0.0093(3)
0.19781(5)	0.19796(8)	0.19779(6)	0.19789(6)	0.19794(6)	0.19789(6)
0.18730(5)	0.18744(8)	0.18738(7)	0.18741(6)	0.18748(6)	0.18751(6)
0.77537(10)	0.77538(16)	0.77572(13)	0.77562(11)	0.77573(11)	0.77579(12)
0.0067(2)	0.0079(3)	0.0069(3)	0.0070(2)	0.0070(2)	0.0070(2)
0.28539(5)	0.28530(8)	0.28519(6)	0.28522(5)	0.28533(5)	0.28532(6)
0.28591(5)	0.28592(8)	0.28571(6)	0.28575(5)	0.28579(5)	0.28577(6)
0.07964(10)	0.07952(16)	0.07954(13)	0.07907(11)	0.07946(11)	0.07937(12)
0.0058(2)	0.0072(3)	0.0062(2)	0.0064(2)	0.0064(2)	0.0067(2)
0.20986(5)	0.20982(8)	0.20980(6)	0.20983(6)	0.20979(6)	0.20975(6)
0.27064(6)	0.27070(9)	0.27072(7)	0.27073(6)	0.27061(6)	0.27057(6)
0.44098(11)	0.44079(17)	0.44095(14)	0.44069(12)	0.44096(12)	0.44099(13)
0.0073(2)	0.0085(3)	0.0077(3)	0.0079(2)	0.0078(2)	0.0080(2)
0.260(2)	0.249(6)	0.261(4)	0.254(4)	0.261(3)	0.259(4)
½ *x*	½ *x*	½ *x*	½ *x*	½ *x*	½ *x*
0.393(4)	0.36(1)	0.390(7)	0.386(8)	0.394(5)	0.396(7)
0.07(1)	0.11(3)	0.06(2)	0.09(2)	0.03(1)	0.07(2)

Determination of ionic distribution

Anionic distribution in the Cruzeiro crystals follows the general preference given by Hawthorne and Henry (1999): the V site (O3) is occupied by OH and the W site (O1) is occupied by F, OH and O^{2-}. When OH + F > 4 apfu, OH in excess is assigned to the O2 site (Federico et al. 1998).

Accurate cation distribution in tourmaline may be determined by combining structural and chemical data (Bosi and Lucchesi 2004). This approach reproduces observed parameters by optimizing cation distribution. Differences between observed and calculated parameters are minimized using the "χ^2" function:

$$\mathrm{F}(X_i) = \frac{1}{n}\sum_{j=1}^{n}\left(\frac{O_j - C_j(X_i)}{\sigma_j}\right)^2$$

where O_j is the observed quantity, σ_j its standard deviation, X_i the variables, i.e., cation fractions at tetrahedral and octahedral sites, and $C_j(X_i)$ the same quantity as O_j calculated by means of X_i parameters. The n O_j quantities taken into account were: mean bond distances (<T-O>, <Y-O>, <Z-O>) and m.a.n. of the T, Y, and Z sites, total atomic proportions given by the microprobe analyses, and constraints imposed by crystal chemistry (total charge and T, Y, and Z site occupancies). As the X site was considered to be populated only by Na, K, Ca, and vacancies, it was not included in the minimization procedure.

Mean bond distances were calculated as the linear contribution of each site cation (X_i) multiplied by its specific bond distance ($\langle T\text{-}O\rangle_i$, $\langle Y\text{-}O\rangle_i$ and $\langle Z\text{-}O\rangle_i$):

$$\langle T\text{-}O\rangle_{calc.} = \Sigma X_i \langle T\text{-}O\rangle_i$$
$$\langle Y\text{-}O\rangle_{calc.} = \Sigma X_i \langle Y\text{-}O\rangle_i$$
$$\langle Z\text{-}O\rangle_{calc.} = \Sigma X_i \langle Z\text{-}O\rangle_i$$

The $\langle Y\text{-}O\rangle_i$ and $\langle Z\text{-}O\rangle_i$ were calculated as the sum of the corresponding cation ionic radii (Table 7) and the anionic one (see next paragraph for details).

Optimal site assignments were determined using a quadratic program solver, and chemical and structural data were satisfactorily reproduced according to the geometrical model of Bosi and Lucchesi (2004). The corresponding site populations are given in Table 8.

RESULTS AND DISCUSSION

Ionic radii at octahedral sites

In tourmaline, the anion dimension is a function of constituent anion radius (Hawthorne et al. 1993): $^{[3]}O$ = 1.36, $^{[4]}O$ = 1.38, $^{[3]}OH$ = 1.34, $^{[3]}F$ = 1.30 Å (Shannon 1976). Variations in anion contents essentially involve W (OH, O) and V (F, OH, O) sites, and, only occasionally, the O2 site (OH, O). The W and V populations affect the mean bond distance around the Z and Y sites. When there is no olenite or buergerite component (for which W = O), the average anion radius (<a.r.>) to the Z site is constant at 1.357 Å, because W = OH. The situation around the Y site is more variable, but in crystals of the schorl-dravite-chromdravite series (Bosi and Lucchesi 2004; Bosi et al. 2004) the anionic radius is almost constant, $\langle^{Y}a.r.\rangle$ = 1.3605(6). As a result, the Z and Y cation radii (<c.r.>) were obtained from the previously refined specific mean bond distances by subtracting the $\langle^{Z}a.r.\rangle$ and $\langle^{Y}a.r.\rangle$ values (Table 7). These cation radii were then used for a first optimization cycle of cation distribution using both the 13 elbaite-schorl crystals from this study and an additional set of seven Mn-rich tourmaline samples (Bosi et al. 2005), but results were not satisfactory. A second optimization cycle was necessary, in which the cation radii were also refined according to the procedure given in Bosi and Lucchesi (2004).

The results reveal that specific cation radii at the Y site are constant in all elbaite-schorl, Mn-rich, and schorl-dravite-chromodravite crystals. Shannon's ionic radius for Li (0.76 Å) does not fit the elbaite-schorl and Mn-rich crystals, for which a value of 0.751 Å was refined (Table 7). Instead, the ionic radii of ^{Z}Al and $^{Z}Fe^{3+}$ were found to increase with respect to those previously obtained for schorl-dravite-chromodravite (^{Z}Al = 0.543 and $^{Z}Fe^{3+}$ = 0.698 Å). The average increase is 0.007(1), leading to ^{Z}Al = 0.550 and $^{Z}Fe^{3+}$ = 0.705 Å. It should be noted that our crystals are characterized by $^{Z}Mg < 0.2$ apfu, whereas the schorl-dravite-

TABLE 5. Mean bond distances (Å) and m.a.n. for the Cruzeiro tourmaline

	66c	61Rda	60fc	62ha	64gh	L4e	61Vbh	L4c	L3h	L4b	L4d	L1v	L1z
<B-O>	1.375(1)	1.3750(8)	1.375(1)	1.3756(9)	1.376(1)	1.378(2)	1.377(1)	1.376(1)	1.376(2)	1.376(2)	1.375(1)	1.376(1)	1.376(1)
m.a.n. B	4.82(5)	4.93(5)	4.88(6)	4.95(6)	4.95(8)	4.87(8)	4.94(6)	4.83(5)	4.88(7)	4.90(6)	4.83(6)	4.78(5)	4.83(6)
<T-O>	1.6167(5)	1.6163(4)	1.6173(5)	1.6172(5)	1.6189(6)	1.6191(8)	1.6208(7)	1.6215(7)	1.623(1)	1.6209(8)	1.6219(7)	1.6231(7)	1.6229(8)
m.a.n. T	13.97(4)	13.98(3)	14.01(4)	13.99(3)	14.00(4)	14.01(5)	14.01(5)	14.01(4)	14.00(6)	13.97(5)	13.94(5)	13.91(4)	13.98(5)
<X-O>	2.672(1)	2.670(1)	2.670(1)	2.671(1)	2.671(1)	2.673(2)	2.683(1)	2.696(2)	2.703(2)	2.699(2)	2.706(2)	2.698(2)	2.699(2)
m.a.n. X	6.53(4)	6.79(4)	8.21(6)	7.80(5)	8.83(7)	10.5(1)	9.72(8)	7.63(7)	7.45(9)	7.28(8)	6.48(6)	8.13(7)	8.01(8)
<Y-O>	2.0000(9)	2.0018(8)	2.0068(9)	2.0114(9)	2.023(1)	2.033(1)	2.038(1)	2.041(1)	2.044(2)	2.042(1)	2.042(1)	2.046(1)	2.046(1)
m.a.n. Y	8.51(3)	8.49(3)	9.84(4)	9.60(3)	11.44(4)	13.75(5)	16.21(6)	19.03(8)	20.7(1)	20.1(1)	20.9(1)	21.05(9)	20.98(12)
<Z-O>	1.9064(6)	1.9064(5)	1.9066(6)	1.9067(6)	1.9070(7)	1.9075(9)	1.9091(8)	1.9120(8)	1.915(1)	1.9148(9)	1.9162(8)	1.9166(8)	1.9169(9)
m.a.n. Z	13.03(3)	13.01(3)	12.97(3)	13.01(3)	13.02(4)	12.96(4)	13.14(4)	13.30(4)	13.43(5)	13.47(4)	13.54(4)	13.47(4)	13.46(4)

Note: Uncertainty in brackets. Estimated error for the mean bond distance is average of standard deviations obtained for single bond distances.

TABLE 6. Chemical composition (wt%), based on EMPA, SIMS, and MS for the Cruzeiro tourmaline

	66c	61Rda	60fc	62ha	64gh	L4e	61Vbh	L4c	L3h	L4b	L4d	L1v	L1z
SiO_2	39.07(14)	38.66(18)	38.40(20)	38.67(15)	37.49(19)	37.27(21)	35.68(18)	35.30(14)	35.25(19)	35.43(20)	34.85(18)	34.70(16)	34.83(17)
TiO_2	–	–	–	–	–	0.28(3)	0.11(2)	0.07(3)	0.23(3)	0.16(3)	0.14(4)	0.22(5)	0.26(3)
B_2O_3*	10.95	10.93	10.73	10.99	10.71	10.45	10.43	9.92	10.09	9.76	9.67	9.60	9.92
Al_2O_3	41.63(17)	41.06(18)	40.08(21)	39.94(16)	38.53(18)	36.74(22)	36.67(20)	35.77(18)	34.93(16)	34.66(21)	34.23(18)	34.33(13)	34.04(19)
FeO*	–	–	1.51(10)	1.08(9)	0.91(11)	5.77(8)	7.14(10)	10.44(20)	13.81(22)	12.86(21)	14.20(20)	14.45(18)	14.25(19)
MnO	0.24(8)	0.22(9)	0.34(7)	0.83(9)	3.32(8)	0.53(11)	1.28(9)	1.41(13)	0.76(11)	0.91(12)	0.38(17)	0.26(11)	0.26(13)
MgO	–	–	–	0.18(10)	–	0.50(7)	–	0.07(7)	0.11(9)	0.09(6)	0.59(10)	1.04(7)	1.22(8)
ZnO	–	–	–	–	–	–	0.94(13)	0.88(16)	0.38(12)	0.59(19)	0.34(14)	0.21(8)	0.24(9)
CaO	0.11(5)	0.24(5)	–	–	0.19(5)	–	0.28(5)	–	0.20(4)	0.05(3)	0.12(5)	0.27(6)	0.40(5)
Na_2O	1.82(6)	1.69(5)	2.20(7)	2.06(5)	2.12(7)	2.67(5)	2.58(6)	2.01(4)	1.86(5)	1.94(8)	1.69(6)	1.99(5)	1.94(7)
K_2O	–	0.05(2)	–	–	0.02(1)	0.02(1)	0.04(2)	0.03(2)	0.04(1)	0.04(2)	0.03(2)	0.05(1)	0.03(2)
Li_2O*	2.11	2.24	1.91	2.14	1.85	1.51	1.16	0.56	0.21	0.30	–	0.20	0.08
F	0.65(11)	0.77(10)	1.25(9)	1.02(11)	1.02(1)	1.47(9)	1.04(9)	0.82(4)	0.45(5)	0.56(3)	0.38(3)	0.38(4)	0.47(4)
H_2O*	3.63	3.47	3.39	3.56	3.29	3.08	3.05	3.01	2.97	3.01	2.96	3.02	2.97
FeO†	–	–	1.51	1.08	0.91	5.77	7.00	7.10	9.87	8.74	9.66	8.09	9.69
Fe_2O_3†	–	–	–	–	–	–	0.16	3.71	4.37	4.57	5.05	7.07	5.07
O=F	–0.27	–0.32	–0.53	–0.43	–0.43	–0.62	–0.44	–0.35	–0.19	–0.23	–0.16	–0.16	–0.20
Total	99.93	99.00	99.28	100.03	99.01	99.68	99.95	99.95	101.10	100.12	99.43	100.56	100.73
Ions calculated on the basis of 31 (O, OH, F)													
Si	6.07(5)	6.06(5)	6.07(5)	6.05(5)	6.02(5)	6.04(5)	5.88(5)	5.88(5)	5.87(5)	5.94(6)	5.91(5)	5.81(5)	5.83(5)
Ti^{4+}	–	–	–	–	–	0.035(4)	0.014(4)	0.009(4)	0.028(4)	0.021(4)	0.018(5)	0.027(6)	0.033(4)
B	2.9(1)	3.0(1)	2.9(1)	3.0(1)	3.0(1)	2.9(1)	3.0(1)	2.9(1)	2.9(1)	2.8(1)	2.8(1)	2.8(1)	2.9(1)
Al	7.62(6)	7.59(7)	7.46(6)	7.37(6)	7.30(6)	7.02(6)	7.12(7)	7.02(7)	6.86(6)	6.85(7)	6.84(6)	6.77(6)	6.72(6)
Fe^{3+}	–	–	0.00(2)	0.00(1)	0.00(1)	0.00(8)	0.02(1)	0.47(2)	0.55(5)	0.58(2)	0.64(3)	0.89(9)	0.64(6)
Fe^{2+}	–	–	0.20(2)	0.14(1)	0.12(1)	0.78(8)	0.96(2)	0.99(2)	1.38(14)	1.23(2)	1.37(3)	1.13(11)	1.36(14)
Mn^{2+}	0.03(1)	0.03(1)	0.05(1)	0.11(1)	0.45(2)	0.07(2)	0.18(2)	0.20(2)	0.11(2)	0.13(2)	0.05(2)	0.04(2)	0.04(2)
Mg	–	–	–	0.04(2)	–	0.12(2)	–	0.02(2)	0.03(2)	0.02(2)	0.15(2)	0.26(2)	0.30(2)
Zn	–	–	–	–	–	–	0.11(2)	0.11(2)	0.05(2)	0.07(2)	0.04(2)	0.03(1)	0.03(1)
Ca	0.018(8)	0.040(8)	–	–	0.032(9)	–	0.049(9)	–	0.036(7)	0.009(5)	0.022(9)	0.048(11)	0.071(9)
Na	0.55(2)	0.52(2)	0.67(2)	0.63(2)	0.66(2)	0.84(2)	0.82(2)	0.65(1)	0.60(2)	0.63(2)	0.56(2)	0.65(2)	0.63(2)
K	–	0.009(4)	–	–	0.005(4)	0.005(4)	0.008(4)	0.007(4)	0.008(2)	0.009(4)	0.007(4)	0.010(2)	0.007(4)
Li	1.32(6)	1.42(6)	1.21(6)	1.35(6)	1.19(6)	0.98(6)	0.77(7)	0.37(7)	0.14(7)	0.20(7)	–	0.14(7)	0.05(7)
F	0.32(5)	0.38(5)	0.63(5)	0.50(5)	0.52(5)	0.75(5)	0.54(5)	0.43(2)	0.23(2)	0.30(2)	0.20(2)	0.20(2)	0.25(2)
OH	3.8(2)	3.6(2)	3.6(2)	3.7(2)	3.5(2)	3.3(2)	3.4(2)	3.3(2)	3.3(2)	3.4(2)	3.3(2)	3.4(2)	3.3(2)
OH+F	4.08	4.01	4.20	4.22	4.04	4.09	3.90	3.78	3.54	3.66	3.55	3.57	3.57
n‡	1.007	1.005	0.999	0.999	1.000	0.995	1.000	0.998	1.000	1.001	1.004	1.000	1.000

Notes: Errors for oxides are standard deviations (in brackets) of repeated analyses on individual crystals. Uncertainties (wt%) for B_2O_3, Li_2O, and H_2O are 0.56, 0.10, and 0.16, respectively. Standard deviation for the ions was calculated by error propagation.

* B_2O_3, Li_2O, and H_2O from SIMS; FeO from EMPA.

† From Mössbauer data, except crystals 60fc, L4e, L3h, L1v, and L1z (estimated by comparison with structural data).

‡ Ratio between total m.a.n. derived from chemical analysis and that obtained by SREF.

chromodravite ones always contain $^{Z}Mg > 0.4$ apfu (Bosi and Lucchesi 2004; Bosi et al. 2004).

Chemical composition

As previously described by Federico et al. (1998), the Cruzeiro tourmaline crystals essentially belong to the elbaite-schorl series. Crystals 66c, 61Rda, 60fc, 62ha, 64gh, L4e, and 61Vbh have a dominant elbaite component, almost double that of rossmannite. Thus, together with elbaite and rossmannite, a third hypothetical end-member, an alkali-free proton-rich elbaite with formula $\square(Li_{1.5}Al_{1.5})Al_6B_3Si_6O_{24}{}^{O2}(O_2OH)^{V}(OH)_3{}^{W}(OH)$, must be considered. This new component reached 12% and is required in order to explain the (OH + F) excess observed in many elbaite crystals (Foit and Rosenberg 1977; Federico et al. 1998) and to clarify the crystal chemistry of the X site (see below). A further confirmation of OH at the O2 site, for elbaites with OH + F > 4 apfu, is given by the bond valences. The bond valence sum (BVS) for the O2 site, calculated using the equation proposed

TABLE 7. Optimized octahedral ionic radii and tetrahedral bond distances (Å)

Cation	<^{Y}c.r.>	<^{Z}c.r.>		<T-O>
Ti^{4+}	[0.605]			
Al^{3+}	0.547	**0.550***	0.543	[1.750]
Fe^{3+}	0.697	**0.705***	0.698	
Fe^{2+}	0.778	0.774		
Mn^{2+}	**0.809**	**0.809**		
Mg^{2+}	0.723	0.720		
Zn^{2+}	[0.740]			
Li^{+}	**0.751**			
Si^{4+}				1.619
B^{3+}				[1.470]

Notes: Uncertainty estimated at ca. 0.001 Å; <^{Z}a.r.> = 1.357 Å for all samples; <^{Y}a.r.> is function of constituent-anion radius.
Bold type = values refined in Cruzeiro and Mn-rich crystals.
Normal type = values obtained from Bosi and Lucchesi (2004).
Square brackets = ionic radii and bond distances from Shannon (1976).
* Valid when ^{Z}Mg < 0.4 apfu.

by Brown and Altermatt (1985), for the 66c, 61Rda, 60fc, 62ha, 64gh, and L4e crystals are: 1.88, 1.89, 1.92, 1.91, 1.96, and 1.98 valence unit (vu), respectively. These values are well below the average value 2.07 vu calculated for O2 in the other Cruzeiro tourmalines (Federico et al. 1998).

The L4c, L3h, L4b, L4d, L1v, and L1z crystals show dominant schorl and minor foitite contents. The Cruzeiro schorl displays Al enrichment associated with $^{Y}Fe^{2+} + {}^{T}Si \leftrightarrow {}^{Y}Al + {}^{T}Al$ substitution (Federico et al. 1998) which, starting from schorl (Hawthorne and Henry 1999), leads to the Al-schorl component. The mechanism $^{T}Si + O^{2-} \leftrightarrow {}^{T}Al + OH$ can be applied to R^{3+}-foitite (MacDonald et al. 1993), thus obtaining a Fe^{3+}-foitite component with OH = 3 apfu, which accounts for the observed Fe^{3+} and OH contents. Together with oxy-foitite (Hawthorne and Henry 1999), these four end-members closely reproduce the observed chemical composition: schorl (Al-schorl + schorl) ranges from 50 to 59%, whereas foitite (Fe^{3+}-foitite + oxy-foitite) ranges from 10 to 44%.

According to Hawthorne and Henry's (1999) classification, the studied tourmalines belong to the alkali group, i.e., X site is dominated by Na (from 0.52 to 0.84 apfu). Moreover, they are distributed among the three fluor-, hydroxy-, and oxy- subgroups. The elbaite crystals lie between the fluor- and hydroxy- subgroups, are O^{2-} free (at the W and V sites) and show OH at the O2 site (up to 0.2 apfu). The schorl crystals always show O^{2-} at the W site and lie between the hydroxy- and oxy- subgroups, except for the L4c crystal (fluor-subgroup).

Lastly, the main substitutional mechanism in the entire elbaite-schorl series is of the dehydroxylation type, described by the equation ($r^2 = 0.99$):

$$^{Y}Fe^{2+} + {}^{Y}Fe^{3+} + {}^{W}O \rightarrow {}^{Y}Li + {}^{Y}Al + {}^{W}(OH + F).$$

Crystal chemistry

B site. In the Cruzeiro crystals, the B content (from 2.8 to 3.0 apfu) may be considered stoichiometric within analytical uncertainty. This is further supported by B-site scattering values (from 4.78 to 4.95) which do not allow unambiguous detection of vacancies (Hawthorne 1996). Moreover, <B-O> values are within the range for B in triangular coordination in tourmaline (Pieczka 1999).

T site. The optimized cation distribution at the T site shows Si, Al, and, occasionally, small amounts of B, consistent with observed <T-O> and m.a.n. values (Table 5). The strong inverse correlation observed between ^{T}Si and ^{T}Al ($r^2 = 0.96$) is due to the previously defined substitutional mechanisms.

X site. The chemical data show that this site mainly contains Na and vacancies. In crystals with (OH + F) ≤ 4, the increase of <X-O> is linearly correlated with $^{X}\square$ content (Fig. 1). However, when (OH + F) > 4, notwithstanding a vacancy content of up to 0.44 apfu, <X-O> is almost constant, ranging from 2.670(1) to 2.673(2) Å. This behavior is also confirmed by Mg-schorl (Bosi and Lucchesi 2004) and elbaite from the island of Elba with OH excess (Bosi et al. 2005). Excess H is bonded to O2 for steric reasons. In the Cruzeiro elbaites, this was confirmed by application of the Bond Valence Model, and excess OH was clearly shown to occupy the O2 position (Federico et al. 1998). This excess H may be located close to O2 and toward O4 and O5. In this way, the expected repulsion among oxygen atoms O2, O4, and O5, which would have caused enlargement of the vacant X-polyhedron, is buffered, thus accounting for the observed constant <X-O> values.

Octahedral sites. The Y site is populated by Al, Li, Fe^{2+}, Fe^{3+}, and minor Mn^{2+} and Mg (Table 8). Major cations show the following linear relations: $^{Y}Fe^{2+} = 3.04 - 1.93{}^{Y}Al$ ($r^2 = 0.90$), $^{Y}Fe^{2+} = 1.28 - 0.89{}^{Y}Li$ ($r^2 = 0.93$), $^{Y}Fe^{3+} = 2.70 - 2.32{}^{Y}Al$ ($r^2 = 0.90$), and $^{Y}Fe^{3+} = 0.66 - 1.01{}^{Y}Li$ ($r^2 = 0.90$).

The substitutions occurring at the Y site are displayed in Figure 2. Starting from nearly stoichiometric elbaite (66c) up to L4e, the schorl → elbaite mechanism is dominant:

$$3{}^{Y}Fe^{2+} \rightarrow 1.5{}^{Y}Al + 1.5{}^{Y}Li \quad (1)$$

Crystal 61Vbh is a "transitional elbaite" which shows Li depletion and an anomalously high Al content; this is due to Al-schorl → elbaite substitution which, as far as the Y site is concerned, may be expressed as:

$$2{}^{Y}Fe^{2+} \rightarrow 0.5{}^{Y}Al + 1.5{}^{Y}Li \quad (2)$$

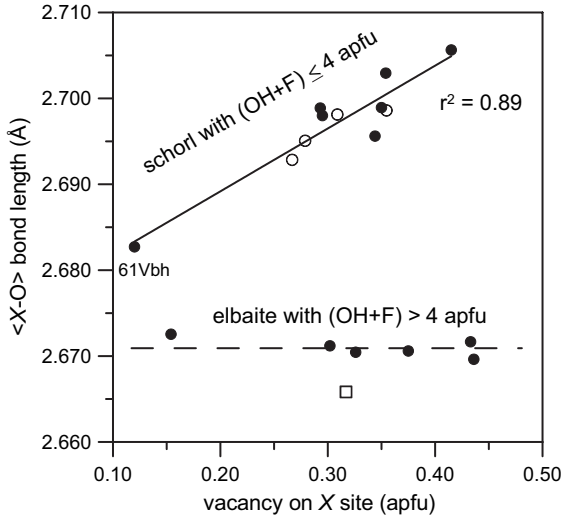

FIGURE 1. Relations between <X-O> and vacancies. Solid circle: elbaite-schorl from Cruzeiro; open circle: Mg-schorl from Cruzeiro (Bosi and Lucchesi 2004); open square: elbaite from the island of Elba (Bosi et al. 2005). Dashed line: guide for the eye.

TABLE 8. Final assigned site populations for the Cruzeiro tourmaline

	66c	61Rda	60fc	62ha	64gh	L4e	61Vbh	L4c	L3h	L4b	L4d	L1v	L1z
X site													
Ca	0.018	0.040	0.000	0.000	0.032	0.000	0.049	0.000	0.036	0.009	0.022	0.048	0.071
Na	0.549	0.515	0.674	0.625	0.661	0.841	0.823	0.649	0.602	0.632	0.556	0.647	0.629
K	0.000	0.009	0.000	0.000	0.005	0.005	0.008	0.007	0.008	0.009	0.007	0.010	0.007
Vacancy	0.433	0.436	0.326	0.375	0.302	0.154	0.120	0.344	0.354	0.350	0.415	0.295	0.293
Y site													
Ti^{4+}	0.000	0.000	0.000	0.000	0.000	0.035	0.015	0.009	0.027	0.023	0.019	0.032	0.034
Al	1.606	1.587	1.514	1.459	1.369	1.170	1.146	1.078	1.001	1.057	1.067	0.865	0.926
Fe^{3+}	0.000	0.000	0.000	0.000	0.000	0.000	0.030	0.329	0.540	0.418	0.404	0.728	0.564
Fe^{2+}	0.000	0.000	0.194	0.118	0.106	0.795	0.861	0.970	1.165	1.139	1.326	1.087	1.228
Mn^{2+}	0.031	0.029	0.043	0.096	0.417	0.072	0.149	0.191	0.098	0.124	0.043	0.032	0.036
Mg	0.000	0.000	0.000	0.044	0.000	0.001	0.000	0.016	0.000	0.000	0.107	0.189	0.130
Zn	0.000	0.000	0.000	0.000	0.000	0.000	0.150	0.108	0.047	0.067	0.033	0.026	0.031
Li	1.363	1.385	1.250	1.282	1.107	0.927	0.649	0.299	0.121	0.172	0.000	0.040	0.050
Σ Y	3.000	3.001	3.000	3.000	3.000	3.000	3.000	3.000	3.000	3.000	3.000	3.000	3.000
Deviation*$_{<Y\text{-}O>}$	0.0001	0.0007	0.0004	0.0006	0.0000	0.0001	0.0001	0.0001	0.0001	0.0002	0.0002	0.0003	0.0001
Deviation*$_{m.a.n}$	0.07	0.01	0.00	0.01	0.00	0.00	0.02	0.00	0.00	0.00	0.00	0.01	0.00
Z site													
Al	6.000	6.000	6.000	5.997	5.987	5.895	5.929	5.860	5.766	5.771	5.720	5.723	5.611
Fe^{3+}	0.000	0.000	0.000	0.000	0.000	0.000	0.000	0.133	0.000	0.165	0.250	0.192	0.095
Fe^{2+}	0.000	0.000	0.000	0.003	0.000	0.000	0.071	0.006	0.203	0.052	0.001	0.023	0.128
Mn^{2+}	0.000	0.000	0.000	0.000	0.013	0.000	0.000	0.000	0.000	0.000	0.000	0.000	0.000
Mg	0.000	0.000	0.000	0.000	0.000	0.105	0.000	0.001	0.030	0.012	0.030	0.062	0.166
Σ Z	6.000	6.000	6.000	6.000	6.000	6.000	6.000	6.000	6.000	6.000	6.000	6.000	6.000
Deviation*$_{<Z\text{-}O>}$	0.0000	0.0004	0.0003	0.0004	0.0000	0.0000	0.0001	0.0001	0.0001	0.0001	0.0001	0.0002	0.0001
Deviation*$_{m.a.n}$	0.03	0.01	0.03	0.00	0.01	0.02	0.01	0.00	0.00	0.00	0.00	0.01	0.00
T site													
Si	5.998	6.000	5.956	5.966	5.996	5.969	5.871	5.893	5.834	5.929	5.883	5.831	5.832
Al	0.000	0.000	0.000	0.000	0.000	0.017	0.103	0.107	0.166	0.071	0.117	0.169	0.168
B	0.003	0.000	0.044	0.034	0.004	0.014	0.026	0.000	0.000	0.000	0.000	0.000	0.000
Σ T	6.000	6.000	6.000	6.000	6.000	6.000	6.000	6.000	6.000	6.000	6.000	6.000	6.000
Deviation*$_{<T\text{-}O>}$	0.0022	0.0027	0.0006	0.0009	0.0000	0.0001	0.0002	0.0001	0.0002	0.0003	0.0003	0.0004	0.0002
Deviation*$_{m.a.n}$	0.03	0.01	0.08	0.04	0.01	0.03	0.07	0.03	0.03	0.02	0.04	0.06	0.01
W site													
F	0.319	0.381	0.626	0.503	0.516	0.754	0.542	0.433	0.235	0.295	0.201	0.201	0.249
OH	0.681	0.619	0.374	0.497	0.484	0.246	0.355	0.346	0.303	0.363	0.347	0.367	0.321
O	0.000	0.000	0.000	0.000	0.000	0.000	0.103	0.221	0.462	0.342	0.452	0.432	0.430
O2 site													
O	2.919	2.987	2.801	2.784	2.960	2.914	3.000	3.000	3.000	3.000	3.000	3.000	3.000
OH	0.081	0.013	0.199	0.216	0.040	0.086	0.000	0.000	0.000	0.000	0.000	0.000	0.000

Notes: For all samples the V site is fully OH-occupied. B content as in Table 6. Atomic frequencies are given to the third decimal point for calculation purposes only.
* Difference, in absolute value, between observed and calculated quantity.

In the L4c to L1z crystals the main substitution is (oxy-foitite) + (Fe^{3+}-foitite) → 2 elbaite which, for the Y site, may be simplified as:

$$3^{Y}Fe^{3+} + {}^{Y}Fe^{2+} \rightarrow {}^{Y}Al + 3^{Y}Li \quad (3)$$

The sum of Equations 1, 2, and 3 gives:

$${}^{Y}Fe^{3+} + 2^{Y}Fe^{2+} \rightarrow {}^{Y}Al + 2^{Y}Li$$

which clearly highlights the fact that depletion of Li is higher than that of Al, and enrichment of Fe^{2+} is higher than Fe^{3+}. Along the elbaite-schorl series, the expansion of <Y-O> is correlated with a decrease in ^{Y}Al content ($r^2 = 0.96$).

The Z site is almost fully occupied by Al, and therefore the Cruzeiro crystals are quite well ordered. In particular, ^{Z}Al is largely dominant in elbaite crystals, while the $^{Z}Fe_{tot} \rightarrow {}^{Z}Al$ substitution ($r^2 = 0.88$) explains the negative linear correlation of <Z-O> with ^{Z}Al ($r^2 = 0.94$) as well as the positive one with $^{Z}Fe_{tot}$ ($r^2 = 0.98$) observed in the schorl crystals.

Unit-cell parameters. In the elbaite-schorl series, the unit-cell parameters are linearly correlated ($r^2 = 0.97$). The relationships between lattice parameters and octahedral sizes are shown in Figure 3. Differing trends distinguish elbaite and schorl compositions, with a change in slope at the "transitional elbaite" 61Vbh. In the elbaite range, the increase in lattice parameters ($\Delta a = 0.097$ and $\Delta c = 0.029$ Å) largely depends on <Y-O> because the

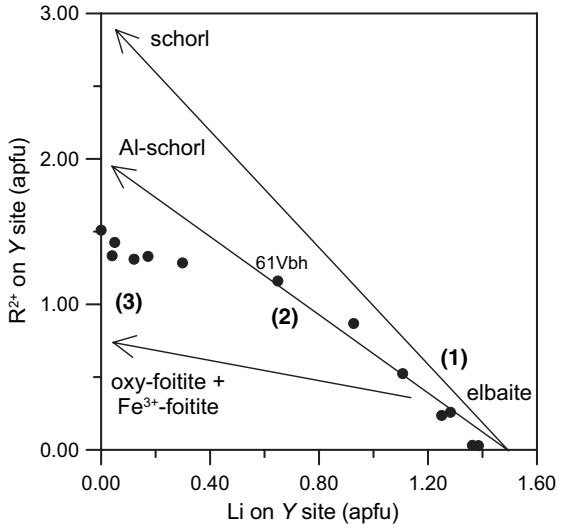

FIGURE 2. Variation from elbaite to schorl by Equations 1, 2, and 3 (see text).

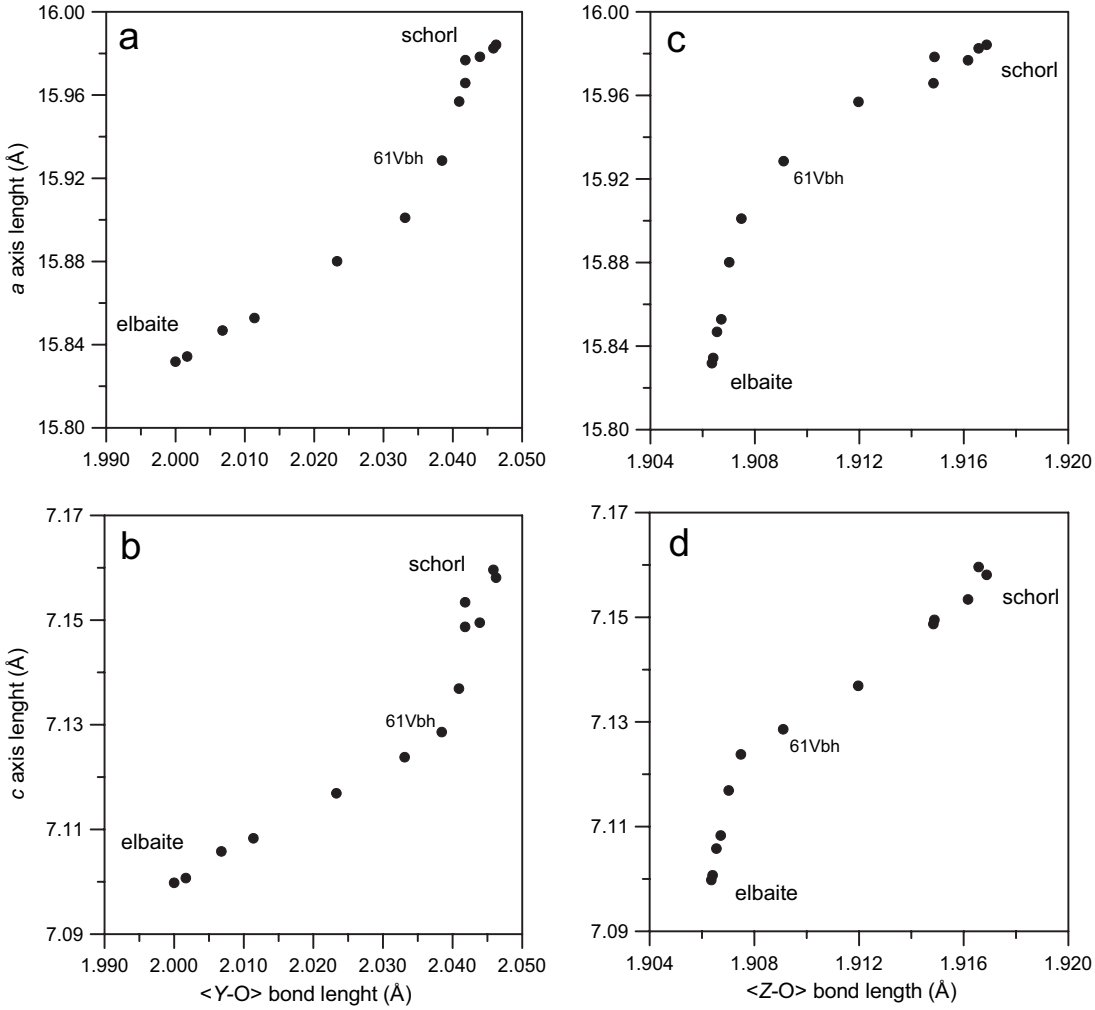

FIGURE 3. Variation of lattice parameters with octahedral sizes. (**a**) *a* vs. <Y-O>; (**b**) *c* vs. <Y-O>; (**c**) *a* vs. <Z-O>, and (**d**) *c* vs. <Z-O>.

substitution $3^{Y}Fe^{2+} \rightarrow 1.5^{Y}Al + 1.5^{Y}Li$ allows large cations to be incorporated, with a net cation radius increase of 0.13 Å, which explains the observed slope. In the same range, <Z-O> changes are very limited, due to nearly constant ^{Z}Al content. Instead, in the schorl range, lattice parameters mainly increase ($\Delta a = 0.056$ and $\Delta c = 0.030$ Å) as a function of <Z-O> rather than <Y-O>. In fact, $^{Z}Fe_{tot} \rightarrow {}^{Z}Al$ substitution results in a net cation radius increase of 0.19 Å, whereas the substitution $3^{Y}Fe^{3+} + {}^{Y}Fe^{2+} \rightarrow {}^{Y}Al + 3^{Y}Li$ gives the smallest increase (0.02 Å).

In conclusion, in the elbaite compositional range lattice parameters are functions of <Y-O>, whereas in the schorl range they are essentially functions of <Z-O>. Notably, along the whole series, both chemical substitutions and size increase of Y are far larger than those of Z. In spite of this, lattice parameters increase with <Y-O> as much as with <Z-O>. This is due to the crucial role of the [ZO_6] polyhedra, which extend along **a** and **c** to form the skeleton of the tourmaline structure. Therefore, any change in Z size affects the entire structure.

ACKNOWLEDGMENTS

The authors are grateful to M. Serracino (CNR, IGAG-Rome) who assisted during the EMP analyses, and G. Walton, who revised the English text. This research was supported by a MURST grant, and carried out within the scientific programs of the Italian CNR, IGG-Rome.

REFERENCES CITED

Andreozzi, G.B., Ottolini, L., Lucchesi, S., Graziani, G., and Russo, U. (2000) Crystal chemistry of the axinite-group minerals: A multi-analytical approach. American Mineralogist, 85, 698–706.

Andreozzi, G.B., Bosi, F., Graziani, G., and Lucchesi, S. (2002) Order-disorder of Al, Mg, Fe^{2+} and Fe^{3+} and site interactions in the borosilicates axinite and tourmaline. Proceedings of 18th General Meeting of the International Mineralogical Association (Edinburgh).

Barton, R. Jr. (1969) Refinement of the crystal structure of buergerite and the absolute orientation of tourmalines. Acta Crystallographica, B25, 1524–1533.

Bosi, F. and Lucchesi, S. (2004) Crystal chemistry of the schorl-dravite series. European Journal of Mineralogy, 16, 335–344.

Bosi, F., Lucchesi, S., and Reznitskii, L. (2004) Crystal chemistry of the dravite-chromdravite series. European Journal of Mineralogy, 16, 345–352.

Bosi, F., Agrosì, G., Lucchesi, S., Melchiorre G., and Scandale, E. (2005) Mn-tourmaline from island of Elba (Italy). I. Crystal chemistry. American Mineralogist, 10, 1661–1669.

Brown, I.D. and Altermatt, D. (1985) Bond-valence parameters obtained from a systematic analysis of the Inorganic Crystal Structure Database. Acta Crystallographica, B41, 244–247.

Burns, P.C., MacDonald, D.J., and Hawthorne, F.C. (1994) The crystal-chemistry of manganese-bearing elbaite. Canadian Mineralogist, 32, 31–41.

Cámara, F., Ottolini, L., and Hawthorne, F.C. (2002) Crystal chemistry of three tourmalines by SREF, EMPA, and SIMS. American Mineralogist, 87, 1437–1442.

Deloule, E., Chaussidon, M., and Allé, P. (1992) Instrumental limitations for isotope ratios measurements with a Cameca IMS 3f ion microprobe: the example of H, B, S, Sr. Chemical Geology, 101, 187–192.

Donnay, G. and Barton, R. Jr. (1972) Refinement of the crystal structure of elbaite and the mechanism of tourmaline solid solution. Tschermaks Mineralogische und Petrographische Mitteillungen, 18, 273–286.

Federico, M., Andreozzi, G.B., Lucchesi, S., Graziani, G., and César-Mendes. J. (1998) Crystal chemistry of tourmalines. I. Chemistry, compositional variations and coupled substitutions in the pegmatite dikes of the Cruzeiro mine, Minas Gerais, Brazil. Canadian Mineralogist, 36, 415–431.

Foit, F.F. Jr. (1989) Crystal chemistry of alkali-deficient schorl and tourmaline structural relationships. American Mineralogist, 74, 422–431.

Foit, F.F. Jr. and Rosenberg, P.E. (1977) Coupled substitutions in the tourmaline group. Contributions to Mineralogy and Petrology, 62, 109–127.

Fortier, S. and Donnay, G. (1975) Schorl refinement showing composition dependence of the tourmaline structure. Canadian Mineralogist, 13, 173–177.

Grice, J.D. and Ercit, T.S. (1993) Ordering of Fe and Mg in the tourmaline crystal structure: The correct formula. Neues Jahrbuch Mineralogie Abhandlungen, 165, 245–266.

Hawthorne, F.C. (1996) Structural mechanisms for light-element variations in tourmaline. Canadian Mineralogist, 34, 123–132.

Hawthorne, F.C. and Henry, D. (1999) Classification of the minerals of the tourmaline group. European Journal of Mineralogy, 11, 201–215.

Hawthorne, F.C., MacDonald, D.J., and Burns, P.C. (1993) Reassignment of cation occupancies in tourmaline: Al-Mg disorder in the crystal structure of dravite. American Mineralogist, 78, 265–270.

Lagarec, K. and Rancourt, D.G. (1998) Recoil: Mossbauer Spectral Analysis Software for Windows, Version 1.0. Department of Physics, University of Ottawa, Ottawa, Canada.

MacDonald, D.J., Hawthorne, F.C., and Grice, J.D. (1993) Foitite, $\square(Al,Fe^{3+})Al_6Si_6O_{18}(BO_3)_3(OH)_4$, a new alkali-deficient tourmaline: Description and crystal structure. American Mineralogist, 78, 1299–1303.

Pieczka, A. (1999) Statistical interpretation of structural parameters of tourmalines: the ordering of ions in the octahedral sites. European Journal of Mineralogy, 11, 243–251.

Shannon, R.D. (1976) Revised effective ionic radii and systematic studies of interatomic distances in halides and chalcogenides. Acta Crystallographica, A32, 751–767.

MANUSCRIPT RECEIVED SEPTEMBER 30, 2004
MANUSCRIPT ACCEPTED FEBRUARY 22, 2005
MANUSCRIPT HANDLED BY GEORGE LAGER